Proceedings of International Conference on Heat Exchanger Fouling and Cleaning - 2011 (Peer-reviewed)
June 05 - 10, 2011, Crete Island, Greece
Editors: M.R. Malayeri, H. Müller-Steinhagen and A.P. Watkinson

DEPOSITION BEHAVIOR OF A BITUMINOUS COAL IN A LARGE PULVERIZED FUEL POWER PLANT

S. Babat[1], J. Maier, G. Scheffknecht, G. Stein-Brzozowka and E. Miller

[1] Institute of Combustion and Power Plant Technology
Pfaffenwaldring 23, D-70569 Stuttgart
Selahattin.Babat@ifk.uni-stuttgart.de

ABSTRACT

In order to understand the mineral transformation and the formation of deposits, analytical methods based on deposit analyses have been developed at the University of Stuttgart, as an enhancement to traditional deposit analysis techniques. The analytical methods were successfully applied to deposits collected from a small-scale and large-scale pulverized power plant.

Fly ashes and deposits were collected in a large-scale pulverized power plant at the super heater level to investigate growth and development of deposits. Emphasis was placed on the chemical characterization of deposits collected on a cooled temperature controlled probe (630-730°C) and an uncooled probe as well as their interpretation regarding fouling and slagging phenomena. The temperature controlled probe was used to investigate the initial layer of deposits while the uncooled probe was used to investigate the outer layer.

Even under oxidizing conditions, several compact iron-rich particles deposited on the cooled deposit. Contrary to the temperature controlled deposit, the uncooled deposit showed a high porosity, a brittle behavior and a high content of SiO_2.

INTRODUCTION

Fouling and slagging are very complex phenomena, which depend upon construction of the boiler, operation parameters and on the fuel properties. The release of inorganic compounds of the fuel during combustion and their transformation into troublesome aerosols, ash particles, and gaseous species could substantially affect the boiler efficiency and the overall economics by the formation of fireside deposits. Ash formed during fuel thermal conversion and deposited on furnace walls and convective pass heat transfer surfaces, acts as a heat transfer resistance and may thereby inhibit heat transfer to the steam cycle. If not removed, deposits may reduce the boiler thermal performance and, in severe cases, completely block flue gas channels and therefore subsequently cause unscheduled boiler shutdowns [1]. The performance of the furnace and the super-heater concerning the conditions of slagging, for the most part, depends on the properties of the initial layer (inner layer) [2]. The initial layer, adjacent to the heat transfer surface usually has a particulate structure depending upon construction of the boiler, operation parameters and on the fuel properties.

In general, the initial deposit layers are rich in small particles that have high levels of flame-volatilized species such as sodium and sulfur. In addition, the initial layers may provide fluxing materials that will cause larger particles to melt. Furthermore layers are dominated by alkali sulphates, chlorides [3] and simple oxides such as CaO, MgO, FeO, Fe_2O_3, Fe_3O_4 and complex silicate phases that are stable in the radiant section of the boiler [4]. The initial layers are generated by small particles (<1 µm) and vapor phase species. These species are characteristically flame-volatilized and condense upon gas cooling in the bulk gas on ash particles or in the gas boundary layer next to the tube. The diffusion mechanisms (such as Fick diffusion and Eddy diffusion) are important with respect to the transport of vapor species and small particles. A mechanism of ash particle transport in the <10 µm size range of particles is thermophoresis. Thermophoresis is a transport force that is produced as a result of temperature gradient in the direction from hot to cold. According to the literature, the transport mechanisms for these initial layers are primarily due to small particle and vapor phase diffusion and thermophoresis. The initial deposit layer provides a sticky surface which is impacted by larger non-sticky particles. The outer surfaces become more insulated from the water cooled steel surface and the temperature of the deposit surface increases [1, 4]. Consequently this results in increasing quantity of liquid phase. The deposit grows further and larger aluminum- and silicon-rich particles are deposited and the deposit will approach the bulk composition of the ash [5]. Once the initial layer has been developed and the heat absorption rate significantly reduced, the deposit can grow to substantial thickness with little further loss in absorption [6].

An understanding of how and why the initial layers of deposit are formed is important for the understanding of the fouling and slagging process. Therefore the objective of this study was to investigate the inner and the outer layer of deposit samples collected during the combustion of a bituminous coal. Modern analytical methods such as ICP, XRD, CCSEM, EMPA were used in order to determine the chemical composition, the particle size and the crystalline phases, which subsequently determine probable mechanisms of formation. Moreover, polished cross-sections of deposits were analyzed in an electron microprobe to characterize the chemical composition, phase identification and chemical distribution of the deposit layers. Particular focus is on the deposit analysis in order to understand the mineral transformation and the formation of the collected deposits (cooled and uncooled). The formation of these deposits will be discussed based on previous works in the literature.

EXPERIMENTAL SECTION

Measurements were conducted at the super heater level in a large-scale pulverized power plant with tangential firing. In order to understand the mineral transformation and the formation of deposits, two different types of deposits were collected to investigate the ash deposition phenomena. A temperature controlled (cooled) probe, as shown in Fig. 1, was used to collect cooled deposits. Thereby, different material rings were mounted on the probe and the temperature of the first ring on the top of the probe was set to a desired temperature that was controlled by an airflow, which was regulated by a controller. The temperatures of the other rings increased linearly up until 100 K; their temperatures were measured by thermocouples. This type of ash deposit-sampling should represent the initial layer. For the investigation of the outer layer of the deposit, an uncooled probe was used in this work.

Fig. 1 Cooled deposits collected by a water and air cooled probe in the super heater level exposed 231 h at a temperature between 990-1113 °C

Uncooled deposits were collected by using a probe that has a high refractory ceramic tube screwed in the front of the probe as illustrated in Fig. 2.

In addition, fly ash sampling, gas measurement and temperature profiles were performed at the super heater level where the deposits were collected. Fuel sample was taken after a roller mill.

Coal Characterization

Ultimate and proximate analyses of the fuel sampled after the roller mill were done. In addition modern analytical methods such as ICP, XRD and CCSEM were performed in order to determine mineral and chemical composition, particle size and the crystalline phases, which subsequently determine probable mechanisms of formation. The particle size distribution of the fuel sample was obtained by a particle size analyzer (Mastersizer 2000) based on laser diffraction.

Fly Ash and Deposits Characterization

ICP analysis was done with fly ash from the super heater level to determine the chemical composition of the bulk ash. In addition particle size distribution of bulk ash was determined.

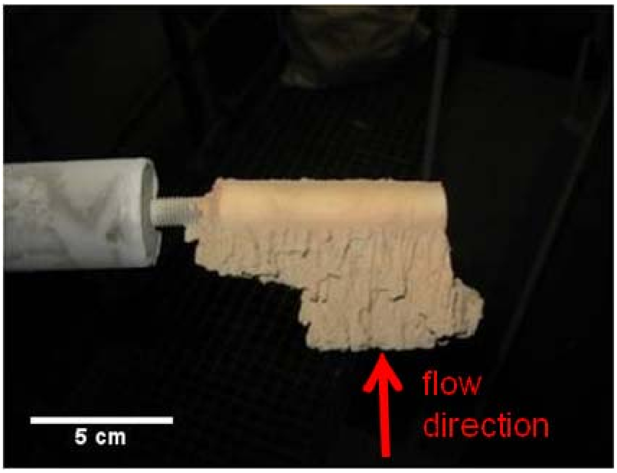

Fig. 2 Uncooled deposit collected by a ceramic tube

EMPA and SEM analysis was performed to analyze chemical composition of different particles on the cooled and uncooled deposits and to investigate the shape of the particles and interaction of the particles (e.g. formation of agglomerates, formation of neck between particles and deformation of particles, etc.).

RESULTS AND DISCUSSION

In the following section the results of the experiments are presented starting with the coal analysis, followed by the fly ash and deposit analyses. This part ends with a discussion of the results and an interpretation based on literature review.

Fuel analysis

Standard coal analysis of the bituminous coal

The ultimate and proximate analyses of the bituminous coal are presented in Table 1. The coal shows a relatively high volatile matter and an average ash content compared to other bituminous coals. In comparison with other bituminous coals, the bituminous coal used in this work has a high amount of acid and a low amount of basic elements in ash. The ash composition leads one to expect a low slagging and fouling tendency.

Particle size distribution

As previously stated the focus of this work was to investigate the formation of inner and outer layers of deposits for enhancing the understanding of the fouling and slagging behavior. This was accomplished not only by standard coal analyses (ultimate, proximate and ash analyses), ash analyses and deposit analyses, but also by the characterization of the particle size distribution by laser diffraction of the milled coal and of the fly ash collected at the super heater level.

The particle size distribution of the milled coal and the fly ash is given in Table 2. The particle diameters D10, D50 and D90 were used to express the particle size distribution of the samples. The values of D50 indicate that 50% of the particles in the sample are smaller than that diameter.

Table 1. Properties of the bituminous coal

Proximate [wt.-% , wf.]	Volatile matter	32.81
	Ash	12.63
	Fixed Carbon	54.56
Ultimate [wt.-% waf.]	C	85.58
	H_{fuel}	5.61
	N	1.65
	S	1.14
	O_{diff}	6.43
Lower heating value [MJ/kg, wf.]	LHV	29.45
Ash composition 815°C [wt.-% ,wf.]	Al_2O_3	22.60
	CaO	0.99
	Fe_2O_3	4.23
	K_2O	2.67
	MgO	0.69
	Na_2O	0.48
	P_2O_5	0.15
	SiO_2	65.80
	SO_3	0.81
	TiO_2	1.68

Table 2. Particle size distribution of the coal after the mill and of the fly ash particles at super heater level

	milled coal	fly ash
d10 [µm]	5.7	2.6
d50 [µm]	35.7	19.7
d90 [µm]	117.3	67.0

CCSEM and XRD analysis of the bituminous coal

Computer Controlled Scanning Electron Microscopy (CCSEM) is used to determine the size, composition and abundance of minerals in coals. In addition to the quantitative mineral analysis in the coal, the occurrence of the minerals as included or excluded mineral can be determined by CCSEM. Included mineral matter, defined to be mineral matter that forms an inorganic entity within the coal structure while an excluded mineral matter, defined as mineral matter which is not attached to the coal mass but is external to it.

Table 3 presents the CCSEM analysis for the investigated bituminous coal. The table can be read as follows: 14 wt.-% of the minerals determined by CCSEM is classified as quartz and 27 wt.-% out of the quartz is found in the particle range between 4.6-10 µm and 22 wt.-% of all the minerals are in the range between 4.6-10 µm.

Kaolinite, K Al-silicate and quartz add up to 70 wt.-% and pyrite, montmorillonite and Si-rich mineral are together 9 wt.-%. The minor minerals and unclassified minerals add up to 20 wt.-%. Mineral inclusions with particle size between 2.2 and 46 µm add up more than 60 wt.-% of the total minerals, while only 9 wt.-% of the mineral matter was in the particle size range smaller than 2.2 µm. About 60 wt.-% of the minerals were greater than 10 µm. The minerals determined by CCSEM were also detected by XRD.

Deposits collection and their behavior

Cooled deposit: As mentioned above the deposits were collected with a temperature controlled probe in a temperature range of 630 to 730 °C. The temperature of the material rings can be controlled as needed. The temperature measured at the sample location was between 990 and 1113 °C. The fly ash-deposition settles down on the cooled metal rings mounted on the cooled probe. After an exposure time of 231 h the probe was removed from the boiler. The outer layer of the cooled deposit showed a loosely powdery ash deposit which was settled on the tube. Very few particles from the deposit were lost when the probe was taken out of the boiler. The outer part of the cooled deposit could be easily removed with a brush contrary to the inner part, which stuck to the tube. As it can be seen in Fig. 1 there is less deposit formation on the rings during the exposure time of 231 h compared to the uncooled deposit shown in Fig. 2, which was collected during a period of only 20 min. Thus, due to the less amount of the cooled deposit, it was not possible to measure the deposit thickness,

Uncooled deposit: Uncooled deposits were collected by using a probe where a ceramic tube is mounted at the top of the tube as illustrated in Fig. 2. The temperature at the location where the probe was inserted was also between 990 and 1113 °C. The uncooled deposit which can be seen in Fig. 2 was collected during a period of only 20 min. Almost 5 cm deposit was grown on the probe in this period of time. This would correspond to a deposition rate of 15 cm/h, if it is assumed that there is no deposit removal due to the erosion, gravity force and thermal stresses. However, when deposit was collected on the uncooled ceramic probe it showed lightly sintered ash particles with a very brittle character. On the upstream tube side, an elliptical- or beard-like-shape was observed. The strength of the deposits barely held the particles together as the deposit sample was removed from the boiler.

Deposits analysis

When the deposits were collected, the samples were embedded in an epoxy resin to keep the deposits stable. Afterwards the samples were cut to the desired size and were embedded in resin again to facilitate their handling in order to improve the results of preparation. The Vector Power head polishing machine from BUEHLER was used to polish the side of interest to its finest.

Mechanical preparation is divided into two operations - grinding and polishing. The grinding was done by using SiC papers of different grain sizes from the largest to the smallest (P60, P120, P180, P320, P400, P1000, P1200). Water was used as a lubricant and a force of 25 N was applied for each grinding steps. For the polishing of the sample a polycrystalline diamond suspension of 6 micrometre, of 3 microns and then 1 micron were used on a polishing cloth. Fig. 3 shows the embedded cooled and uncooled deposits which are prepared for EMPA analysis.

Table 3. CCSEM mineral size and composition distribution

Mineral species	wt.-%	Particle size (micrometer)							
		0.5-1	1-2.2	2.2-4.6	4.6-10	10.-22	22.-46	46.-100	>100
Quartz	14	0	6	12	27	12	20	21	2
Kaolinite	34	3	8	11	20	11	21	24	2
Montmorillonite	3	2	1	2	17	21	20	37	0
K Al-silicate	22	1	7	9	22	10	19	28	5
Fe Al-silicate	1	1	24	25	18	0	8	23	0
Pyrite	3	1	0	3	19	11	19	48	0
Si-Rich	3	0	6	14	30	13	25	11	0
Minor minerals	2	4	15	14	27	13	18	9	0
Unclassified	18	3	7	6	18	9	19	25	12
Totals	100	2	7	10	22	11	20	25	4

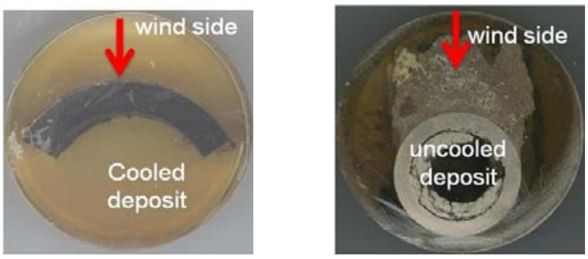

Fig. 3 Cooled (left) and uncooled (right) deposit after embedding for analysis

BSE-analysis of the cooled and uncooled deposits

Fig. 4 shows the backscatter electron (BSE) images of the cooled and uncooled deposits. The BSE detector allows materials with different compositions to be imaged as different grayscale contrasts. The backscattering increases with increasing average atomic number, which leads to brighter ranges in the image. Image A and B in Fig. 4 show the particle distribution of the cooled deposits, which were controlled at a surface temperature at 690 and 730 °C. Several areas at cooled deposits were analyzed and on every investigated area irregular molten iron-rich and spherical particles were observed. Numerous fine gray particles deposited on the surface of the sample. Some particle especially the bright particles indicated the iron-rich particles agglomerated with each other and surrounding the fine particles and some larger Al-silicate fly ash particles.

Due to the few cenospheric particles found here (which indicate the release of a gas in some particles during the combustion), it can be concluded that the particles were melted before sticking on the probe surface. The deformed shape of the iron-rich particles is caused by collision and indicates that iron-rich particles had low viscosity during impact. This assumption is confirmed by the particles which build partial bridges between different particles. Many spots and several maps have been performed to investigate the composition of the cooled deposits, as will be discussed later.

For the cooled deposit it can be summarized that several large iron-rich particles create a compact deposit by surrounding mainly smaller particles compared to the uncooled deposit. A similar appearance to the deposits sampled here was also reported by Laursen et al. for air and water cooled probes [7].

Image D shows the inner part and image C shows the central part of the uncooled deposits in Fig. 4. For the uncooled deposits less spherical and bright particle with big spaces between the particles, hence big porosity of the deposit is observed. The fly ash particles are very loosely bonded and there are no neck formations between the particles. As can be seen from the image C and D, the porosity of the uncooled deposit is very high. For the investigation of the composition of the uncooled deposits many spots and several maps have been performed and will be discussed later.

cooled deposits uncooled deposits

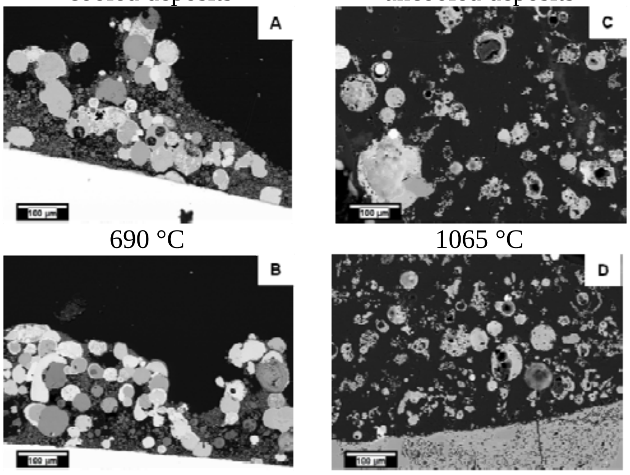

690 °C 1065 °C

730 °C 1065 °C

Fig. 4 BSE images of the cooled (left) and uncooled deposits (right) with a scale of 100 µm.

Iron-Map

The EMPA analyses were used to obtain compositional information in the deposits using characteristic X-rays. In order to investigate the different elements in the samples EMPA-Map were implemented for the 10 main elements (Al, Ca, Fe, K, Mg, Na,P, Si, S and Ti). Maps were generated to interpret the composition of the cooled and uncooled deposits. Fig. 5 shows the corresponding EMPA map for iron. It can be clearly seen that iron-rich particles were mainly on the cooled deposit probe. Only a few iron particles were found on the uncooled deposit probe. The brighter the particles are, the higher the content of iron.

Mainly aluminium and silicon were observed in the uncooled deposits as can be seen in Fig. 6. In addition to the iron-rich particles, Al-silicates were also detected in the cooled deposits.

Fe-distribution cooled deposits Fe-distribution uncooled deposit

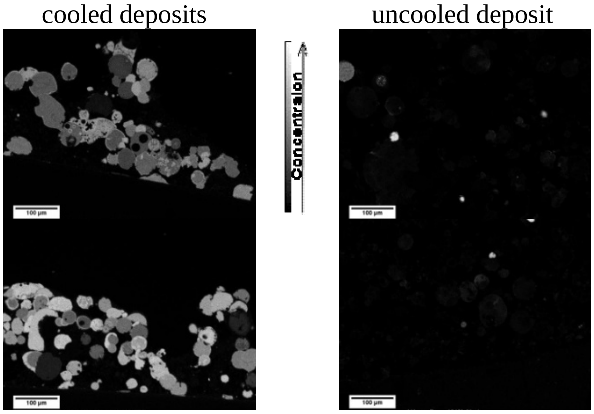

Fig. 5 Iron distribution in the cooled (left) and uncooled (right) deposits.

Fig. 7 show the potassium, calcium, magnesium and sodium distribution in the cooled deposits controlled at surface temperature at 730°C and uncooled deposit in the central part. Almost the same amount of potassium and sodium was determined in the cooled and uncooled deposit. The amount of calcium in the cooled deposit was slightly more than in the uncooled deposit.

Al- and Si-distribution cooled deposits

Al- and Si-distribution uncooled deposits

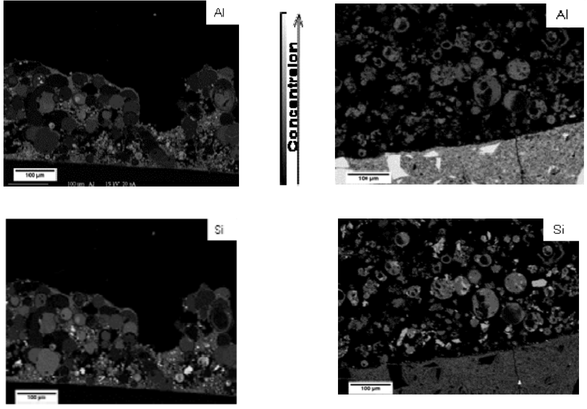

Fig. 6 Aluminium and silicon distribution in the cooled and uncooled deposits.

With the concentration bar in Fig 5, Fig. 6 and Fig. 7 qualitative conclusions could be drawn about the amount of elements in the deposits. In order to draw quantitative conclusions about the particle composition and to underline the preceding results several spots were chosen for analyzing the chemical composition by EMPA analysis.

In addition to the map analyses, 64 spots were performed for the cooled and 88 spots for the uncooled deposit. Fig. 9 provides one example of how the spots have been evaluated for the cooled deposits. Fifty spots are drawn in the Fig. 8 that were subsequently analyzed by EMPA in order to determine the elemental composition. Points chosen ensured that different phases are considered. The elemental compositions achieved by spot analyses were converted to the equivalent oxide composition in order to be able to compare with standard ash analysis.

The spot analyses confirm the iron-rich particles in the cooled and the absence of them in the uncooled deposits. Iron-oxide content of 4.23 wt.-% for the fuel ash generated in the laboratory and 4.1 wt.-% for the fly ash and 4.0 wt.-% for the uncooled deposits were determined by ICP.

With the EMPA spot-analysis, an average iron-oxide content of 64.7 wt.-% for the cooled deposit and of 4.21 wt.-% for the uncooled deposits were determined.

The average content of the other element-oxides such as potassium, calcium, magnesium and sodium are shown in Table 4.

Fig. 9 shows the average spot analysis of cooled and uncooled deposits compared with the ash content generated in the laboratory at 815 °C and of a sample collected with a particle suction probe where the ash deposit probe was inserted between 990 and 1113 °C. The laboratory ash and the fly ash were analyzed with Inductively Coupled Plasma-Optical Emission Spectrometry (ICP-OES).

For further interpretation of the deposit-analysis, the data from the spot-analysis were illustrated on a ternary diagram which can be used to visually examine the deposits chemical properties.

K-, Ca-, Mg- and Na-distribution of the cooled deposit

K-, Ca-, Mg- and Na-distribution of the uncooled deposit

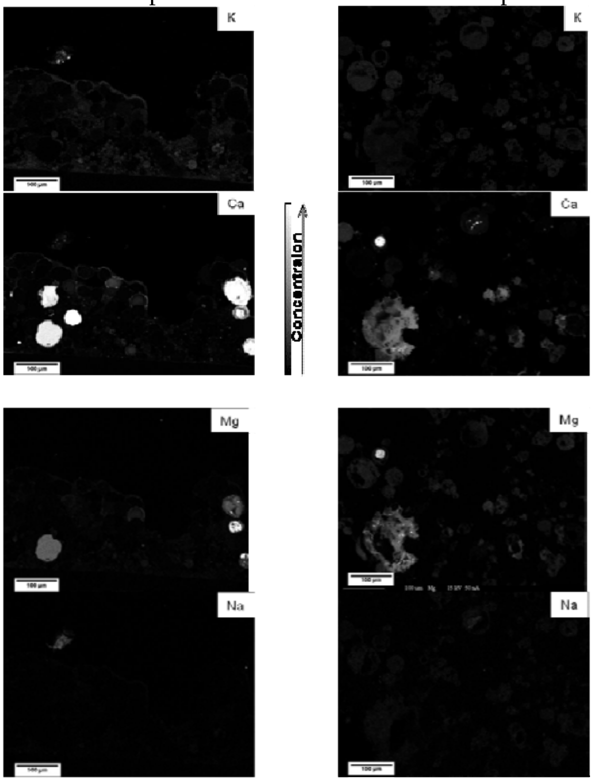

Fig. 7 Potassium, calcium, magnesium and sodium distribution in the cooled deposits controlled at surface temperature at 730°C and uncooled deposit (central part).

Table 4. The average chemical composition of the cooled and uncooled deposit determined by spot analyses.

Elementoxide [wt.-%]	uncooled	cooled
Al2O3	28,0	10,7
CaO	2,1	2,7
Fe2O3	4,2	64,7
K2O	2,5	0,4
MgO	1,0	0,9
Na2O	0,2	0,1
P2O5	0,2	0,5
SiO2	60,0	19,3
SO3	0,0	0,2
TiO2	1,7	0,5

The three main oxides which make up the composition of the deposits investigated in this work are SiO_2, Al_2O_3 and Fe_2O_3. Therefore normalized ash composition (SiO_2 +

Al_2O_3 + Fe_2O_3=100 %) of the particles found on the cooled and uncooled deposits are illustrated in Fig.10 based on a ternary diagram. All the data from the spot analysis are displayed in this diagram. The enrichment of iron-particles in the cooled deposits and the high amount of Al-silicates in the uncooled deposits can be seen clearly.

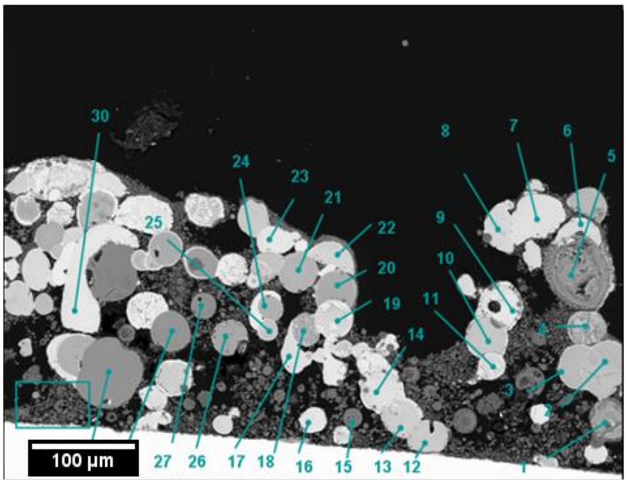

Fig. 8 Example how the spots have been conducted on a cooled and uncooled probe

The element maps and spot analyses show iron-rich particles on the cooled deposits. Due to the thermal gradient between the flue gas and the tube surface of the cooled deposit there is a selective deposit of iron rich particles.

Due the existence of the melt in the iron-rich particle, the particles in the flue gas that reach the surface of the cooled deposit tend to stick to it. The reason might be that the iron-rich particles contacted alumino-silicates which lead to coalescence and lead to low melting point of these particles for the given conditions in the boiler. From the CCSEM analysis and XRD analysis it can be concluded that iron is mainly present in the form of pyrite in this investigated coal.

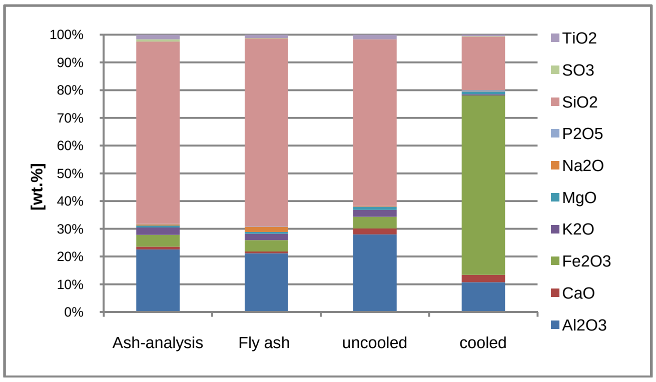

Fig. 9 Average spot analyses of cooled (64 Spots) and uncooled (88 Spots) deposits compared with the fly ash and the ash generated in the laboratory.

As stated in the literature according to McLennan et al. [8] iron mineral transformations were expected to be most affected by combustion stoichiometry. The decomposition of pyrite (FeS_2) to pyrrhotite ($Fe_{1-x}S$) starts at a temperature of 800 to 900 K [9].

Further, Mc Lennan et al. reported that excluded pyrite decomposes to pyrrhotite, and then oxidizes from the surface inward to produce a molten FeO-FeS phase at 1353 K. These transformations are dependent on both temperature and oxygen concentration. Under oxidizing conditions the molten phase will oxidize to magnetite and hematite. It remains as FeO-FeS phase under reducing conditions.

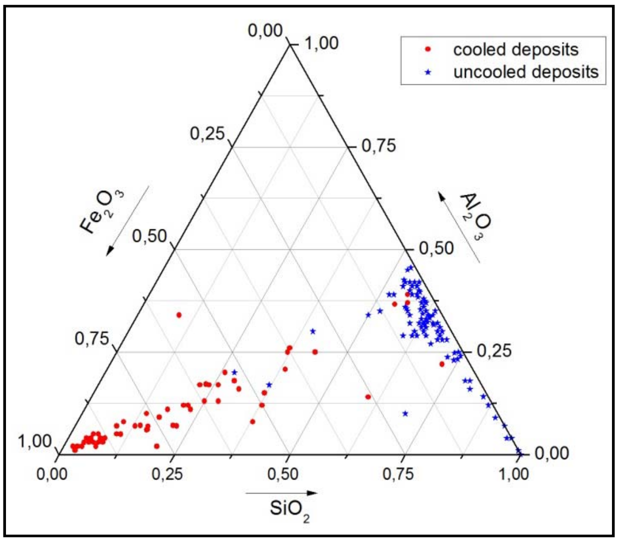

Fig. 10 SiO_2 - Al_2O_3 - Fe_2O_3 ternary diagram of the cooled and uncooled deposit

For the included pyrite mineral, it is reported by McLennan et al. that included pyrite may behave as excluded pyrite if there is no contact with alumino-silicates, though oxidation will be delayed by char combustion. Included pyrite that contacts alumino-silicate minerals will form two phase FeS/Fe-glass ash particles, with incorporation of iron into the glass proceeding as the FeS phase is oxidized. This delay in glass formation is expected to be accentuated by reducing conditions.

Gas measurement and temperature profile were performed at the super heater and at the burner level. At the burner level a minimum amount of 1.1 vol.-% O_2 was measured 5 m distance from the wall along the central line axes of the burner. It must be mentioned that only single points were measured at three measurements ports that may not be representative of all actual conditions in the boiler. It is believed that reducing conditions also occur, which affect the transformation of excluded and included pyrite.

At the burner level gas temperature about 1430°C and particles temperature between 1400 -1500°C was measured by Sabel in previous works performed at IFK in this boiler [10]. On the super heater level where the deposits were collected, an O_2 concentration between 2.5 to 4.5 vol.-% and a temperature of 990 to 1113 °C was measured. The average temperature was about 1065 °C. CCSEM and XRD results identified significant amount of pyrite in the bituminous coal. The pyrite mineral was both included (2 wt.-%) and excluded (1 wt.-%) as can be seen in Table 5.

Table 5 CCSEM analyses of the bituminous coal showing the amount of included and excluded minerals

	included	excluded	total
	wt.-%		
unclassified	9	9	18
Minor minerals	3	1	4
Pyrite	2	1	3
Fe Al-silicate	0	1	1
K Al-silicate	10	12	22
Kaolinite	18	16	34
Quartz	7	7	14
Montmorillonite	2	1	3
Si-Rich	1	2	3

About 59 wt.-% of the included pyrite found in the bituminous coal was in the size range of 46 to 100 µm. Included pyrite smaller than 46 µm add up to 41 wt.-%.

About 32 wt.-% of the excluded pyrite found in the bituminous coal was in the size range of 46 to 100 µm. Excluded pyrite smaller than 46 µm add up to 68 wt.-% . The iron-rich particles found in the cooled deposits are in a range of about 15 to 100 µm as shown in Fig. 11.

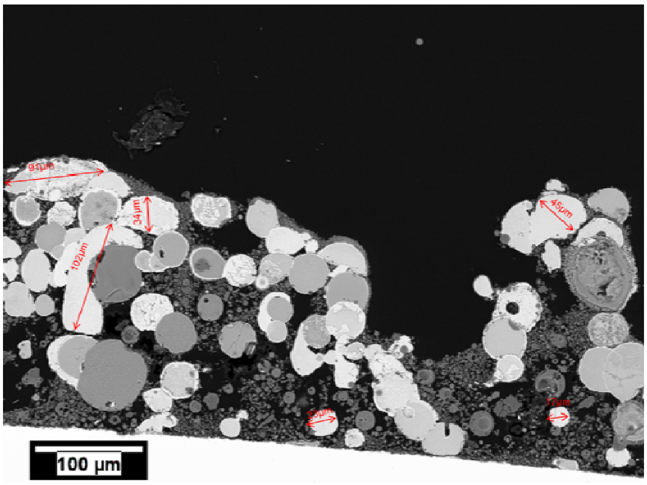

Fig. 11 particle size of the iron-rich particles found in the cooled deposits as example.

As mentioned previously and investigated by McLennan et al., the oxidation of included pyrrhotite will not proceed to high extent until complete burnout of the char. The investigations in [8, 9] indicate that the included pyrite in the char tend to stick to the super heater walls due to the existence of a FeO or Fe-O-S melt, which contacts alumino-silicates and lead to a low melting point.

As the samples were collected at super heater area, the particles have attained a certain residence time in the boiler. It is assumed that most of the iron rich particles observed in the cooled deposit come from the included pyrite. Some excluded pyrite particle will be oxidized to magnetite or hematite before it reaches the super heater surface area and the adhesiveness will be much lower because of the high melting point of magnetite (1811 K) and hematite (1838 K). Due to the oxidizing conditions the deposited iron-rich particles are oxidized further to magnetite and hematite.

The surface temperature of the cooled probe is too low to sustain melting of the initial deposit layer, which consist primarily of small, lightly sintered particles and a few larger adhered particles as can be seen in Fig. 4. Softening and even melting of the deposit on the cooled probe is not expected for this investigated coal at the sampling location under conditions mentioned above.

In the real process after a certain time in a boiler the deposit grows, its surface temperature increases, and eventually reaches the melting temperature of the low temperature melting deposit material. The increase in the deposit surface temperature causes the softening and even melting of the deposit [1, 11, 12]. This kind of deposit should be represented by the uncooled deposit. The surface temperature of the uncooled deposit probe is equal to the flue gas temperature at the place where the uncooled deposit was sampled. Due to the high temperature (1338 K) at the surface of the uncooled deposit probe melting temperature of the low temperature melting deposit material is reached and therefore a softening and even melting of the deposit could be most likely formed. Due to the existence of melt, most of the fly ash particles that reach the surface tend to stick to it, causing the outer deposit layer to have a composition similar to the bulk fly ash composition as can be seen from the analysis in Fig. 9.

Shedding behavior of the investigated deposits

Ash deposits can be removed from boiler heat transfer surfaces using artificially induced methods, e.g. by soot blowers, but deposits can also be removed without any external influence.

Spontaneous shedding may be caused by: erosion, gravity force and thermal stresses. Artificial shedding is caused by operationally induced erosion, and mechanically and thermally induced stresses within the deposit [1].

The inner layer of initial layer deposit which was investigated in this work was strongly attached to the metal surface, so that even with a blade it was difficult to remove the deposit formed on the cooled sample. Therefore it is assumed that with the common industrial shedding technique as the soot blower it will not be possible to remove this inner layer of the initial layer totally. In contrast to the cooled deposit the uncooled deposit with its high porosity might be removed by a soot blower when the right Peak Impact Pressure, PIP (local stagnation pressure in a sootblower jet) is chosen. Beside the understanding of deposit growth and the formation of the deposit, further efforts has to be put into the analysis of the deposit strength, the porosity and the sintering conditions when different quality of coals are applied.

CONCLUSIONS

The following conclusions can be drawn concerning the ash formation mechanisms during pulverized coal combustion of this bituminous coal and the formation of the deposits.

(1) The collections of the deposits with a cooled and uncooled probe proved to be successful to investigate

the inner and outer layer of a deposit and to improve the understanding of deposits growth as well as the understanding of fouling and slagging phenomena.

(2) On the cooled deposit several large iron-rich particles create a compact deposit by surrounding mainly smaller particles compared to the uncooled deposit. As the oxidation of included pyrrhotite will not proceed to any great extent until complete burnout of the char, the included pyrite in the char tend to stick to the super heater walls due to the existence of a FeO or Fe-O-S melt, which contacts alumino-silicates and lead to a low melting point.

(3) According to literature, the transport mechanisms for the initial layers are primarily due to small particle and vapor phase diffusion and thermophoresis. Within this work several large-particles (>10 µm) were observed. Therefore inertial impact transport mechanisms played a dominant role for the formation of the initial layer of the deposits. The results cannot confirm that the large fly ash particles played a higher role in formation of the bulk sintered layer on top as reported in literature [13].

(4) The uncooled deposit shows almost no iron-rich particles and high porosity compared to the cooled deposit. Due to the high temperature (1338 K) at surface of the uncooled deposit probe, melting temperature of the low temperature melting deposit material is reached and therefore a softening and even melting of the deposit occurred. Due to the existence of melt, most of the fly ash particles in the flue gas that reach the surface tend to stick to it, causing the outer deposit layer to have a composition similar to the bulk fly ash composition.

(5) In contrast to the cooled deposit, the uncooled deposit with its high porosity might be totally removed by soot blowers when the right PIP (Peak Impact Pressure) is chosen.

ACKNOWLEDGEMENTS:

This work was performed under KW21-programm, which was funded by EnBW (Energie Baden-Württemberg AG, Germany) and the State Baden-Württemberg in Germany. EnBW is acknowledged for support during the full-scale trials. Institut für Mineralogie und Kristallchemie, University of Stuttgart, is acknowledged for support with EMPA and XRD techniques.

NOMENCLATURE

BSE	Back-Scattered Electron
CCSEM	Computer Controlled Scanning Electron Microscope
EMPA	Electron Microprobe Analysis
ICP-OES	Inductively Coupled Plasma-Optical Emission Spectrometry
PIP	Peak Impact Pressure
Vol.-%	volume percent
waf.	water ash free
wf.	water free
wt.-%	weight percent
XRD	x-ray diffraction

REFERENCES

[1] A. Zbogar, F. Frandsen, P. A. Jensen, P. Glarborg: Shedding of ash deposits. *Progress in Energy and Combustion Science*, Vol. 35, pp. 31-55, 2009.

[2] A. N. Alekhnovich, Natalja V. Artemjeva, V.V. Bogomolov, V. I. Shchelokov V.G. Petukhov: Prognosis of slagging and fouling properties of coals based on widely available data and results of additional measurements. *Impact of Mineral Impurities in Solid Fuel Combustion*, edited by Gupta et al. Kluwer Academic / Plenum Publishers, New York, pp. 455-469, 1999.

[3] KH. Andersen: Deposit formation during coal- straw co-combustion in a utility pf-boiler. *PhD Thesis*. Lyngby: DTU, ISBN 87-90142-43-8; 1998.

[4] D.E. Thornock, R.W. Borion: Developing a Coal Quality Expert: Combustion and Fireside Performance Characterization Factors. *Topical report on coals from public service of Oklahomas's northeaster station*, 1992.

[5] Z. Ma, F. Imam, P. Lu, R. Sears, L. Kong, A.s.Rokanuzzaman, D.P. McCollor, S.A.Benson.: A comprehensive slagging and fouling prediction tool for coal-fired boilers and its validation/application. *Fuel Processing Technology*, Vol. 88, pp. 1035–1043 , 2007.

[6] R. W. Bryers: Factors Critically Affecting Fireside Deposits in Steam Generators. *Impact of Mineral Impurities in Solid Fuel Combustion*, edited by Gupta et al. Kluwer Academic / Plenum Publishers, New York, pp. 105-131, 1999.

[7] K. Laursen and F. J. Frandsen: Classification System for Ash Deposits Based on SEM Analyses. *Impact of Mineral Impurities in Solid Fuel Combustion*, edited by Gupta et al. Kluwer Academic / Plenum Publishers, New York, pp. 205-216, 1999.

[8] A. R. McLennan, G.W. Bryant, B.R. Stanmore, T.F. Wall.: Ash Formation Mechanisms during pf Combustion. *Energy & Fuels*, Vol. 14, No. 1, 2000.

[9] S. Srinivasacher and A. A. Boni: A kinetic model for pyrite transformations in a combustion environment. *Fuel*, Vol 68, pp. 829-836, 1989.

[10] T. Sabel: Betriebsoptimierung von Kohlekrafwerksfeuerungen durch Experiment und Simulation. *Doktorarbeit*, Stuttgart, ISBN 3-8322-3223-0, 2004.

[11] L. Hansen: Melting and sintering of ashes. *PhD Thesis*,. Lyngby: DTU, ISBN 87-90142-31-4; 1998.

[12] G. Couch: Understanding slagging and fouling in pf combustion. *IEA Coal*, Research, Report No. I EACR/72, 1994.

[13] L. A. Hansen, F. J. Frandsen, H. S. Sorensen, P. Rosenberg, K. Hjuler, K. Dam-Johansen: Ash Fusion and Deposit Formation at Straw Fired Boilers. *Impact of Mineral Impurities in Solid Fuel Combustion*, edited by Gupta et al. Kluwer Academic / Plenum Publishers, New York, pp. 341-355, 1999.